Lasing dynamics of neutral nitrogen molecules in femtosecond filaments

Pengji Ding, Eduardo Oliva, Aurélien Houard, André Mysyrowicz, and Yi Liu

PHYSICAL REVIEW A **00**, 003800 (2016)

Lasing dynamics of neutral nitrogen molecules in femtosecond filaments

Pengji Ding,[1,2] Eduardo Oliva,[3] Aurélien Houard,[1] André Mysyrowicz,[1] and Yi Liu[1,*]

[1]*Laboratoire d'Optique Appliquée, ENSTA ParisTech, CNRS, Ecole Polytechnique, Université Paris-Saclay, 828 Boulevard des Maréchaux, 91762 Palaiseau cedex, France*

[2]*School of Nuclear Science and Technology, Lanzhou University, 730000 Lanzhou, China*

[3]*Instituto de Fusión Nuclear, Universidad Politécnica de Madrid, 28006 Madrid, Spain*

(Received 26 February 2016; published xxxxxx)

We investigate the dynamics of cavity-free lasing from neutral nitrogen molecules in femtosecond laser filaments. An important difference of intensity and temporal duration is observed between backward and forward lasing, in both amplified spontaneous emission and seed-amplification regimes. Numerical simulations based on a nonadiabatic Maxwell-Bloch model reproduce well the observations, and attribute these differences to the finite gain lifetime and the traveling excitation nature of this gas laser.

DOI: 10.1103/PhysRevA.00.003800

I. INTRODUCTION

Coherent emission from the atmosphere is attracting intense attention because of its potential in remote sensing applications [1–8]. Traditional optical remote sensing systems for probing the atmosphere rely on collecting backward-scattered incoherent light from targets in the atmosphere to detectors on the ground, a technique hindered by low efficiency and poor directionality. Availability of a light source which emits coherent light in the backward direction from a certain point in the sky back towards a ground-based detector could have a great impact on the efficiency and precision of optical remote sensing techniques [9]. Several possible approaches have been proposed for implementing a free-space mirrorless laser source emitting in the backward direction [1–3,5–14]. One of the most promising approaches so far is through two-photon dissociation and subsequent resonant two-photon excitation of neutral oxygen or nitrogen atoms by deep-UV laser pulses. However, the strong absorption of deep-UV pump laser pulse in air ultimately limits the distance at which this type of laser can be pumped [1,3,6]. This restriction disappears with a pump laser in the visible or IR region.

Recently, Mitryukovskiy and co-workers demonstrated that the filament plasma column created by intense femtosecond laser pulse at 800 nm in air can act as an optical amplifier and give rise to lasing at 337.1-nm wavelength in backward directions [11]. Stimulated emission at this wavelength corresponds to a transition between levels $C\,^3\Pi_u^+ \rightarrow B\,^3\Pi_g^+$ in the triplet manifold of the neutral nitrogen molecule. Amplification takes place only if the infrared (IR) laser pulse is circularly polarized [11]. In the presence of external seeding around 337.1 nm in both backward and forward directions, the emission was enhanced by orders of magnitude [12,13]. Based on a study on the sideway fluorescence, inversion of population between states $C\,^3\Pi_u^+$ and $B\,^3\Pi_g^+$ responsible for optical gain has been attributed to the following scenario [see Fig. 1(a)] [14]. The intense filamentary pulse of peak intensity, $I = 1.5 \times 10^{14}\,\mathrm{W/cm^2}$, liberates free electrons from nitrogen and oxygen molecules through a high-field tunneling process [11,15]. The energy of the free electrons left after the passage of the pulse depends sensitively on the laser polarization. For a linearly polarized pump pulse at 800 nm, most free electrons are left with low kinetic energy. By contrast, with circularly polarized light, the electrons have a peak in their energy distribution at $E = 2U_p = 14.5\,\mathrm{eV}$ where $U_p = e^2/c\varepsilon_0 m_e(I/2\omega_0^2)$ [Fig. 1(b)]. Fortuitously, this energy is optimal to promote a nitrogen molecule from its ground state to state $C\,^3\Pi_u^+$ via impact collision and to achieve thereby inversion of population with respect to $B\,^3\Pi_g^+$. We have previously reported seed-amplified lasing in pure nitrogen in the forward as well as the backward direction, wherein the backward geometry pump and seed pulses are counterpropagating [12]. However, the presence of oxygen with a concentration in excess of 10% led to a quenching of lasing [11,13].

We now routinely observe seed-amplified emission in air in the forward direction using a pump laser pulse of a few millijoules of energy and 50 fs duration (see Fig. 2); however, this is not yet the case in the backward direction. The main reason is the pronounced asymmetry of the lasing intensity between backward and forward geometries in favor of the latter. This is regrettable since backward lasing is particularly useful for long distance atmospheric diagnostics. It is therefore important to understand in detail the origin of this asymmetry in order to envision strategies allowing backward lasing in air.

To this purpose, we have measured the temporal dynamics of the amplified spontaneous emission (ASE) and of externally seeded lasing at 337.1-nm wavelength in a filament in pure nitrogen, both in the forward and backward directions. These emissions were examined in the time domain with time-resolved techniques [11–13]. Significant differences in pulse duration and intensity are observed for ASE versus seeded lasing and for copropagating versus counterpropagating pump-seed geometries, features which are unexpected. We apply to our present case a theoretical model that successfully explained the collisional-induced amplification of XUV high-order harmonics injected into a plasma column. This model, which takes into account the pump-seed geometry and the initial free-electron energy distribution, reproduces the observed dynamics. It explains the strong lasing signal asymmetry in the forward versus backward gain, which originates from the short lifetime of optical gain and the traveling excitation nature of the filament amplifier. It also shows that an analysis relying solely

*yi.liu@ensta-paristech.fr

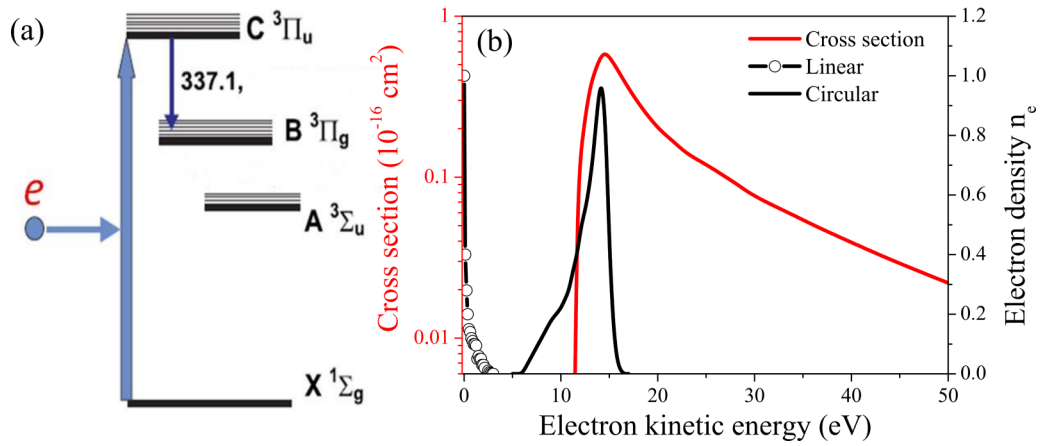

FIG. 1. (a) Schematic energy levels of the neutral nitrogen molecules. Collisional excitation of the ground-state ($X\,^1\Sigma_g$) N_2 molecules results in population inversion between the third excited state ($C\,^3\Pi_u^+$) and the second excited state ($B\,^3\Pi_g^+$). (b) Cross section of the collisional excitation to the $C\,^3\Pi_u^+$ state (red) and the electron energy distribution in the filaments pumped by circularly polarized femtosecond pulse (black line) and the linearly polarized one (black line–dot).

on rate equations would be insufficient to treat the results. Instead, full consideration of the medium polarization and of the nonadiabatic excitation process is necessary.

II. EXPERIMENTAL RESULTS

In the experiments, femtosecond laser pulses (wavelength centered at 800 nm, pulse duration of 45 fs, repetition rate of 100 Hz, and maximum pulse energy of 16 mJ) delivered by a commercial laser system (Thales, Alpha 100), were split into three replicas, *a*, *b*, and *c*. The time delays between these pulses were controlled by mechanical optical delay lines. For the creation of the nitrogen filament amplifier, a circularly polarized femtosecond pulse of ~9 mJ (replica *a*) was focused by a convex focal lens with $f = 1$ m into a nitrogen-gas-filled chamber. Both backward and forward ASEs at 337.1 nm from the filamentary plasma with a length $l \sim 30$ mm were recorded. To obtain the seeding pulse at 337.1 nm, the second harmonic of pulse *b* was generated in a 1-mm-thick BBO crystal and then focused into a 20-mm-thick fused silica sample. A narrow spectral bandwidth (~10 nm bandwidth) of the emerging broadband continuum was selected with an interference filter around 337 nm. More technical details can be found in [12]. The seed pulse could be injected into the plasma in both directions. To characterize the pulse duration, the forward 337-1 nm ASE or amplified lasing radiation was focused together with the third 800-nm pulse replica *c* on a 2-mm-thick type-I BBO crystal cut specially at 50.7°, to efficiently produce a sum frequency generation (SFG) signal at 238 nm wavelength. By recording the sum frequency signal at 238 nm as a function of the time delay between the 337.1-nm lasing signal and the weak 800-nm probe pulse *c*, the temporal profile of the 337.1-nm lasing pulse is obtained.

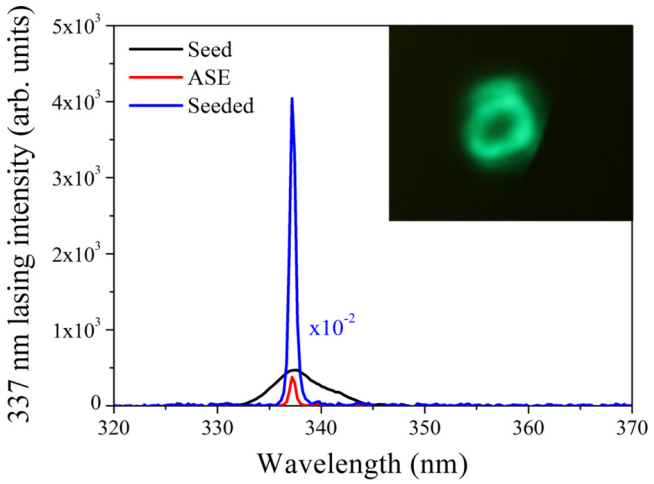

FIG. 2. Amplified spontaneous emission (red) and seeded emission (blue) obtained in ambient air in the forward direction. The ~9-mJ circularly polarized femtosecond laser pulse was focused by an $f = 1$ m lens in atmospheric air. The inset presents the profile of the forward ASE obtained in pure nitrogen gas.

We first present the optical gain dynamics of the 337.1-nm lasing emission measured in the pump-seed copropagation configuration. By measuring the seed amplification as a function of relative delay between pump and weak seed pulse, the temporal profile of gain can be probed. The result shown in Fig. 3 reveals a rapid gain buildup time of ~5 ps, and a slow decay time of ~35 ps. The duration of optical gain [full width at half maximum (FWHM)] is about $\tau_g = 13$ ps. Now we turn to the temporal profile of the stimulated radiation in the forward direction. The measured temporal structure of the forward ASE and seeded amplified emission are presented in Fig. 4(a). The 337.1-nm ASE pulse shows a buildup time of 17 ps and a slow decay up to 53 ps, with a full width at half maximum duration of ~20 ps. In contrast, the seeded emission presents a much shorter rise time of ~3 ps and a duration of 4 ps. The seeded lasing pulse precedes the ASE by about 20 ps. The peak intensity is 50 times higher than for ASE, in good agreement with previous reports [12,13]. Note the slight temporal modulation structures with a period of about 11 ps apparent for both ASE and seeded emission, a feature related to the quantum beating effect that will be discussed later.

The temporal profile of the backward externally seeded 337.1-nm lasing pulse measured with the cross-correlation method is shown in Fig. 4(b). It was normalized to its

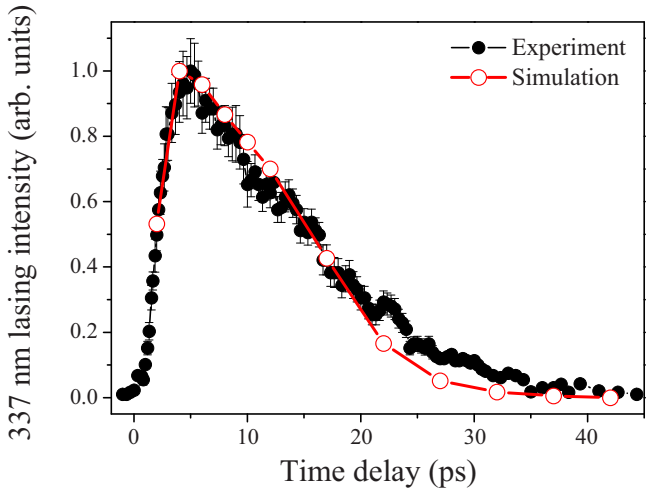

FIG. 3. Experimental (solid black dots) and simulated (red circles) results of the gain dynamics of 337.1-nm lasing emission with 7.5-mJ pump pulse energy under 1 bar of nitrogen gas.

counterpart in the forward direction. The radiation peak is delayed by 14 ps with respect to the seed pulse and a significant intensity modulation of period 11 ps is now obvious. The envelope of the backward seeded 337.1-nm lasing pulse gives a FWHM duration of ∼15 ps. If we just concentrate on the strongest pulse following the seed pulse, it has a width (FWHM) of 4 ps. We have also found, by measuring the lasing pulse energy with a photodiode, that the backward seeded emission was about 150 times weaker than the forward one under the same excitation conditions. The backward 337.1-nm ASE lasing signal was too weak to be measured by the cross-correlation method. We therefore turned to a Michelson interferometer to estimate its pulse duration by measuring the interference fringe visibility between two 337.1-nm ASE pulse replicas as a function of their relative delay. The interference pattern was captured by an intensified charge-coupled device (iCCD) (Princeton Instruments, PI-MAX). A periodic modulation of the fringe contrast with a period of ∼11 ps is well apparent [see Fig. 4(c)], indicating that the ASE is also composed of multiple peaks in the temporal domain, similar to the seeded emission presented in Fig. 4(b). It yields a coherence time of ∼120 ps, corresponding to a duration of 85 ps, as assuming a Fourier transform-limited ASE pulse.

III. THEORETICAL MODELING

In order to understand the different temporal dynamics of the forward and backward 337.1-nm emission observed in experiments, we adapted the one-dimensional time-dependent Maxwell-Bloch code DEEP-ONE [16,17] to our current case, following the lines of [18,19]. This code, originally developed to study the amplification of soft x rays ($\lambda = 10-40$ nm) in hot, dense plasma ($n_e > 10^{18}$ cm^{-3}, $T_e > 10-100$ eV), solves the paraxial wave equation for the electric field in the slowly varying envelope approximation,

$$\frac{\partial E_\pm}{\partial t} \pm c\frac{\partial E_\pm}{\partial z} = \frac{i\omega_0}{2}\left[\mu_0 c^2 P_\pm - \left(\frac{\omega_p}{\omega_0}\right)^2 E_\pm\right], \quad (1)$$

where E_+, E_- are the electric fields propagating in the forward and backward directions, respectively; P_+, P_- are the corresponding polarization densities of the medium; c is the light velocity in vacuum; ω_0 is the frequency of the electric field; ω_p is the free-electron plasma frequency; and μ_0

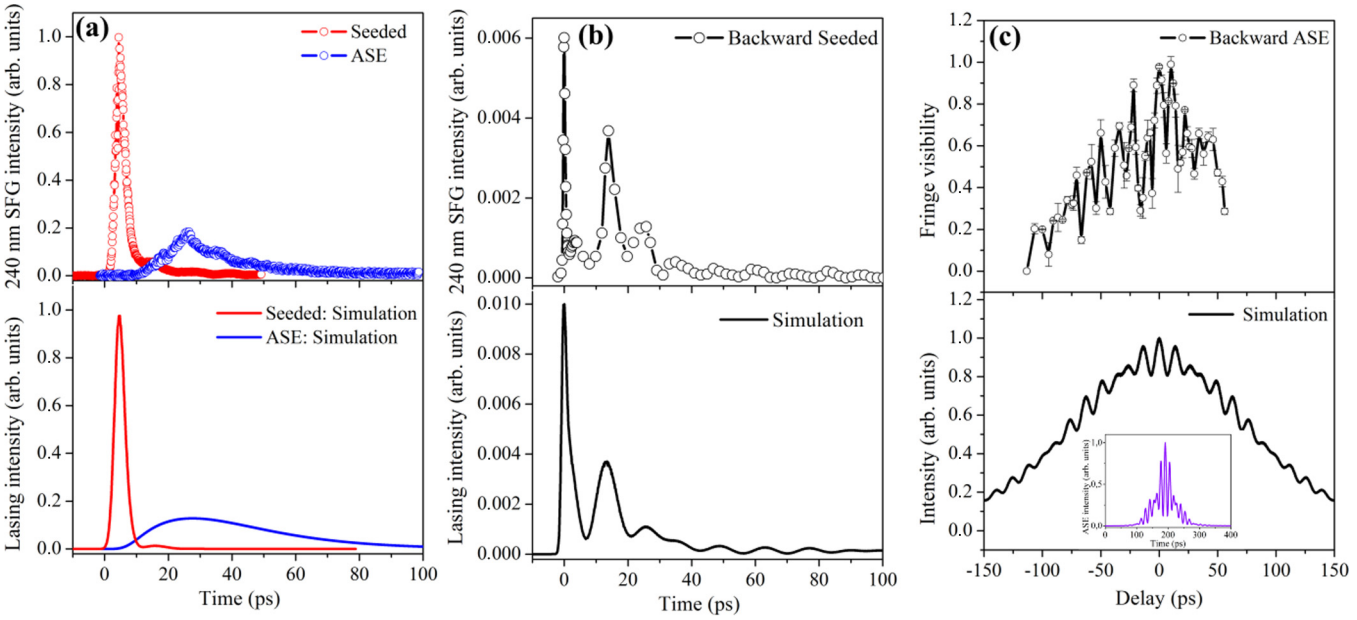

FIG. 4. (a) Experiment (upper panel) and simulation (lower panel) results of temporal profiles of forward 337.1-nm ASE lasing pulse (blue line) and externally seeded 337.1-nm lasing pulse (red line). The signal for the 337-nm ASE lasing pulse is enlarged by ten times for better comparison. (b) Experiment and simulation results of temporal profile of backward externally seeded 337.1-nm lasing pulse. (c) Experiment and simulation results of the autocorrelation trace of backward 337.1-nm ASE. The inset in the lower panel shows the simulated temporal profile of the backward 337.1-nm ASE.

is the vacuum permeability. Equation (1) is enhanced with a constitutive relation derived from Bloch equations,

$$\frac{\partial P_\pm}{\partial t} = \Gamma - \gamma P_\pm - \frac{i z_{ul}^2}{\hbar} E_\pm (N_u - N_l), \tag{2}$$

where Γ is a stochastic source term with vanishing correlation time modeling the spontaneous emission [20,21]; γ is the depolarization rate due to collisions; z_{ul} is the corresponding dipole matrix element (that can be deduced from Einstein's A coefficient); and N_u, N_l are, respectively, the population of the upper and lower levels of the lasing transition. Since the seed duration (∼100 fs) is shorter than the typical collision time of the plasma (∼ps), the adiabatic approximation is no more valid [22] and the full differential equation [Eq. (2)] must be used to describe the evolution of the polarization. These populations are computed by using rate equations,

$$\frac{\partial N_i}{\partial t} = \sum_k C_{ki} N_k \pm \Im(E^* P) \frac{1}{2\hbar}, \tag{3}$$

where $i = u,l$ and C_{ki} are the collisional (de)excitation and radiative deexcitation rates. These rates are computed from the cross sections reported in [23].

The evolution of electron density and temperature are computed using the model presented in [18,19], with the initial electron temperature for circular laser polarization obtained in [14,24]. The electron temperature T_e and the vibrational temperature T_v are given, respectively, by

$$\frac{3}{2}\frac{\partial N_e T_e}{\partial t} = -Q_c N_a N_e \left(1 - \frac{T_v}{T_e}\right), \tag{4}$$

$$\frac{3}{2} N_a \frac{\partial T_v}{\partial t} = Q_c N_a N_e \left(1 - \frac{T_v}{T_e}\right), \tag{5}$$

where N_e is the electron density; N_a the neutral density; and Q_c is the cooling rate, that for $T_e < 2$ eV is given analytically by the following formula:

$$Q_c \approx 3.5 \times 10^{-8} \exp\left(-\frac{5}{3T_e}\right) + 6.2 \times 10^{-11} \exp\left(-\frac{1}{3T_e}\right). \tag{6}$$

Since the initial electron temperature of 16 eV cools in less than 6 ps to a value lower than 2 eV, the value of Q_c is extrapolated for $T_e > 2$ eV.

The electron density N_e and positive N_p and negative N_n ion densities are given by

$$\frac{\partial N_e}{\partial t} = \nu_{\text{ion}} N_e - \beta N_p N_e - \eta N_e, \tag{7}$$

$$\frac{\partial N_n}{\partial t} = \eta N_e - \beta_{np} N_n N_p, \tag{8}$$

$$N_p = N_e + N_n, \tag{9}$$

where ν_{ion} is the collisional ionization rate, β is the electron-ion recombination rate, β_{np} is the ion recombination rate, and η the attachment coefficient. The following analytical approximations, obtained from [18], are used to calculate the aforementioned parameters; i.e.,

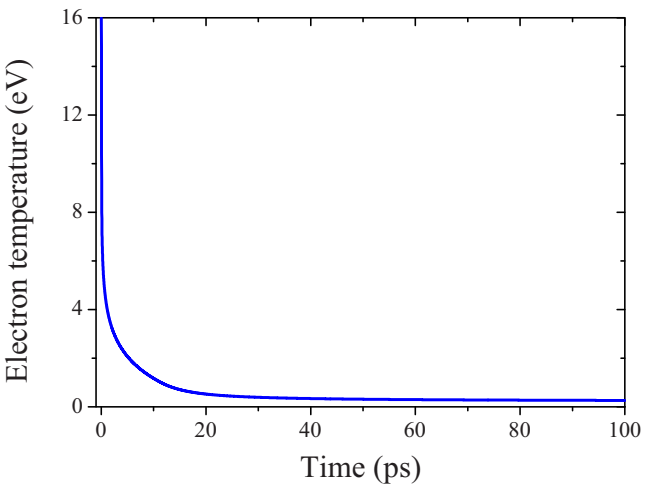

FIG. 5. Temporal evolution of the electron temperature along 100 ps.

$$\nu_{\text{ion}} = \nu_{\text{ion}}(N_2) + \nu_{\text{ion}}(O_2); \tag{10}$$

$$\nu_{\text{ion}}(X) = \nu_X \left(\frac{T_e}{U_X}\right)^{3/2} \left(\frac{U_X}{T_e} + 2\right) \exp\left(-\frac{U_X}{T_e}\right),$$
$$X = \text{N}_2, \text{O}_2; \quad U_{\text{N}_2} = 15.6\,\text{eV}; \quad U_{\text{O}_2} = 12.1\,\text{eV};$$
$$\nu_{\text{N}_2} = 7.6 \times 10^{11}\,\text{s}^{-1}; \quad \nu_{\text{O}_2} = 10^{11}\,\text{s}^{-1}; \tag{11}$$

$$\beta\left(\frac{\text{cm}^3}{\text{s}}\right) \approx 1.5 \times 10^{-8} T_e^{-0.7}, \quad \text{for} \quad T_e < 0.1\,\text{eV}; \tag{12}$$

$$\beta\left(\frac{\text{cm}^3}{\text{s}}\right) \approx 2.0 \times 10^{-8} T_e^{-0.56}, \quad \text{for} \quad T_e > 0.1\,\text{eV}; \tag{13}$$

$$\eta[\text{s}^{-1}] = \alpha_2 N_a + \alpha_3 N_a^2; \tag{14}$$

$$\alpha_2\left[\frac{\text{cm}^3}{\text{s}}\right] = 2.75 \times 10^{-10} T_e^{-0.5} \exp\left(-\frac{5}{T_e}\right); \tag{15}$$

$$\alpha_3\left[\frac{\text{cm}^3}{\text{s}}\right] = 1.5 \times 10^{-32} T_e^{-1} \exp\left(-\frac{0.052}{T_e}\right). \tag{16}$$

IV. NUMERICAL SIMULATION RESULTS AND DISCUSSION

With this model, we performed numerical simulation on the optical gain dynamics. As shown in Fig. 3, the results agree well with the experiments. To understand the ultrafast gain buildup (∼5 ps), we plot the temporal evolution of electron temperature in Fig. 5. The filament has an initial electron density of $N_e = 2 \times 10^{-16}\,\text{cm}^{-3}$ and electron temperature of $T_e = 16$ eV. As shown in the figure, the free electrons cool in the first picoseconds of evolution, due to collisions with neutrals. When the temperature is low enough, the collisional excitation pumping is no longer effective, which therefore leads to a rapid buildup of the gain.

Now we turn to the temporal dynamics of the forward emission. The forward ASE starts from spontaneous emission spanning all the gain duration due to the long lifetime of the upper level of the transition $\tau_u \approx 40$ ns. Amplification and

saturation effects shorten its duration. After passing through 3 cm of plasma, the ASE pulse has a duration (FWHM) of 44 ps, which agrees with our observations [see Fig. 4(a)]. In the external-seeding case, the evolution of the temporal structure of the seed pulse is mainly driven by its initial spectral profile, related to its duration and the linewidth of the transition, dominated by collisions (i.e., a Lorentzian line). The mismatch between the linewidth of the seed pulse and that of the transition triggers the creation, during the first centimeter, and subsequent amplification of a retarded wake pulse [16,22]. When the wake is intense enough, saturation effects reduce its duration until it attains the value of 4.5 ps (FWHM) after propagating through a 3-cm-long filament plasma, again in agreement with the experiment results [see Fig. 4(a)].

Figure 4(b) (lower panel) shows the simulated temporal evolution of the seeded backward emission. Note that the seed and the IR pump pulses enter the plasma from opposite sides, at $t = 0$ ps. Thus, the seed propagates without amplifying until it meets the IR pump in the middle of the filament ($t = 50$ ps). From this point on, the seed is amplified. At the exit of the filament amplifier, the simulation predicts a moderately amplified seed pulse, followed by a wake radiation extending over more than 60 ps, in good agreement with our experiment observations. We would like to point out that this kind of wake emission has been widely observed in the simulation of x-ray amplification in gas plasma [22].

Backward 337.1-nm ASE is much weaker than in the forward case. This is due to the particular geometry of longitudinal pumping. When the spontaneous emission photons propagate in the same direction as the IR pump beam, they interact continuously with a newly created population inversion. On the contrary, in the case of backward ASE, where the ASE counterpropagates with respect to the IR pump beam, the population inversion experienced by the spontaneous emission photon is depleted gradually by the forward ASE that follows the IR pump pulse. In fact, due to the short lifetime of the gain $\tau_g = 13$ ps, the effective amplification length for a spontaneous photon propagating in the backward direction is $l = c\tau_g = 4.2$ mm, which is much less than the 30 mm geometrical length of the plasma filament. After propagating through the 30 mm of N_2 plasma, the pulse duration (FWHM) of the backward ASE is found to be 77 ps, in good agreement with the autocorrelation measurement [see Fig. 4(c)].

What is the origin of the temporal modulation of the lasing observed mainly in the backward geometry? Actually, the lasing line at 337.1 nm, corresponding to the P branch of the $C\,^3\Pi_u^+ \rightarrow B\,^3\Pi_g^+$ transition, is composed of three finely separated branches P_1, P_2, and P_3, due to the interaction between orbital angular momenta and spin [25,26]. The separation between these lines is about 0.33 Å [25], which is beyond the resolution of our spectrometer. The fast collisional excitation process brings the molecules in a coherent superposition of the three branches. An intensity modulation in the temporal domain is then expected due to quantum beating between them. The corresponding temporal modulation period T can be expressed as $T = \lambda_0^2/(c\Delta\lambda)$, where $\lambda_0 = 337.1$ nm is the central wavelength of lasing emission, c is the light speed, and $\Delta\lambda = 0.033$ nm is the wavelength separation of the three branches. Therefore, one obtains $T = 11.5$ ps, in good agreement with the experiment result. Due to the employment of the slowly varying envelope approximation, we are treating the field envelope, not the laser field. As a result, the beating effect cannot directly appear in our Maxwell-Bloch simulations. Thus, we postprocessed our electric field data assuming an interference effect between sublevels to examine if the experimental oscillations were caused by the beating. When the arbitrary phases between the three fields are correct, the position of experimental maxima and minima are retrieved. The simulation results agreed well with the experimental ones, as shown in Fig. 4.

How far are we from obtaining a backward lasing from filaments in air? Our results help define a strategy to reach this goal. The small ratio between backward and forward ASE signal is due to the difference in optical gain path length. It is clear that the effective optical gain length must be increased. This can be achieved along the lines suggested in Ref. [9] by generating a series of aligned filaments. The weak backward ASE from the most remote filament would be amplified in successive steps by crossing the other filaments downstream. Another necessity is to reduce the quenching effect of oxygen molecules. We are presently investigating approaches towards that goal.

V. CONCLUSION

In summary, we have performed experimental measurements and numerical simulations of the temporal dynamics of the bidirectional 337.1-nm lasing pulse from filaments in nitrogen gas pumped by circularly polarized femtosecond laser pulses. The emission in both the ASE and externally seeded regimes was examined with time-resolved techniques. The 337.1-nm ASE pulse in the backward direction has a pulse duration around 85 ps, much longer than that of the forward one (20 ps), and a much weaker peak intensity. In both forward and backward directions, the seeded emission presents a shorter pulse duration and a much enhanced radiation intensity compared to the corresponding ASE. Numerical simulations based on a nonadiabatic Maxwell-Bloch equation agree well with the experimental results and reveal that this difference originates from the traveling excitation scheme of a pump laser and the limited lifetime of optical gain. These results provide valuable temporal information concerning the 337.1-nm radiation from free-space nitrogen-gas plasma pumped by circularly polarized 800-nm femtosecond laser pulses, which can find important applications in lasing-based stand-off spectroscopy in the atmosphere.

ACKNOWLEDGMENTS

We acknowledge the support from Spanish MINECO through the Plan Nacional research program, Grant No. ENE2012-32108, and the People Programme (Marie Curie Actions) of the European Union's Seventh Framework Programme (FP7/2007-2013) under REA Grant Agreement No. 627191, project Dagon.

[1] A. Dogariu, J. B. Michael, M. O. Scully, and R. B. Miles, Science **331**, 442 (2011).
[2] A. J. Traverso, R. Sanchez-Gonzalez, L. Yuan, K. Wang, D. V. Voronine, A. M. Zheltikov, Y. Rostovtsev, V. A. Sautenkov, A. V. Sokolov, S. W. North, and M. O. Scully, Proc. Natl. Acad. Sci. USA **109**, 15185 (2012).
[3] A. Laurain, M. Scheller, and P. Polynkin, Phys. Rev. Lett. **113**, 253901 (2014).
[4] J. Yao, B. Zeng, H. Xu, G. Li, W. Chu, J. Ni, H. Zhang, S. L. Chin, Y. Cheng, and Z. Xu, Phys. Rev. A **84**, 051802(R) (2011).
[5] D. Kartashov, S. Ališauskas, G. Andriukaitis, A. Pugžlys, M. Shneider, A. Zheltikov, S. L. Chin, and A. Baltuška, Phys. Rev. A **86**, 033831 (2012).
[6] A. Dogariu and R. B. Miles, in *Frontiers in Optics 2013—Laser Science XXIX, Orlando, Florida, 2013* (Optical Society of America, Washington, DC, 2013).
[7] V. Kocharovsky, S. Cameron, K. Lehmann, R. Lucht, R. Miles, Y. Rostovtsev, W. Warren, G. R. Welch, and M. O. Scully, Proc. Natl. Acad. Sci. USA **102**, 7806 (2005).
[8] Q. Luo, W. Liu, and S. L. Chin, Appl. Phys. B **76**, 337 (2003).
[9] P. N. Malevich, R. Maurer, D. Kartashov, S. Aliauska, A. A. Lanin, A. M. Zheltikov, M. Marangoni, G. Cerullo, A. Baltuka, and A. Puglys, Opt. Lett. **40**, 2469 (2015).
[10] Y. Liu, Y. Brelet, G. Point, A. Houard, and A. Mysyrowicz, Opt. Express **21**, 22791 (2013).
[11] S. Mitryukovskiy, Y. Liu, P. Ding, A. Houard, and A. Mysyrowicz, Opt. Express **22**, 12750 (2014).
[12] P. J. Ding, S. Mitryukovskiy, A. Houard, E. Oliva, A. Couairon, A. Mysyrowicz, and Y. Liu, Opt. Express **22**, 29964 (2014).
[13] J. Yao, H. Xie, B. Zeng, W. Chu, G. Li, J. Ni, H. Zhang, C. Jing, C. Zhang, H. Xu, Y. Cheng, and Z. Xu, Opt. Express, **22**, 19005 (2014).
[14] S. Mitryukovskiy, Y. Liu, P. Ding, A. Houard, A. Couairon, and A. Mysyrowicz, Phys. Rev. Lett. **114**, 063003 (2015).
[15] P. B. Corkum, Phys. Rev. Lett. **71**, 1994 (1993).
[16] E. Oliva, P. Zeitoun, M. Fajardo, G. Lambert, D. Ros, S. Sebban, and P. Velarde, Phys. Rev. A **84**, 013811 (2011).
[17] Y. Wang, S. Wang, E. Oliva, L. Li, M. Berrill, L. Yin, J. Nejdl, B. M. Luther, C. Proux, T. T. T. Le, J. Dunn, D. Ros, Ph. Zeitoun, and J. J. Rocca, Nat. Photonics **8**, 381 (2014).
[18] P. Sprangle, J. Peñano, B. Hafizi, D. Gordon, and M. Scully, Appl. Phys. Lett. **98**, 211102 (2011).
[19] J. Peñano, P. Sprangle, B. Hafizi, D. Gordon, R. Fernsler, and M. Scully, J. Appl. Phys. **111**, 033105 (2012).
[20] O. Larroche, D. Ros, A. Klisnick, A. Sureau, C. Möller, and H. Guennou, Phys. Rev. A **62**, 043815 (2000).
[21] S. Chandrasekhar, Rev. Mod. Phys. **15**, 1 (1943).
[22] I. R. Al'miev, O. Larroche, D. Benredjem, J. Dubau, S. Kazamias, C. Möller, and A. Klisnick, Phys. Rev. Lett. **99**, 123902 (2007).
[23] T. Tabata, T. Shirai, M. Sataka, and H. Kubo, At. Data Nucl. Data Tables **92**, 375 (2006).
[24] D. Kartashov, S. Ališauskas, A. Pugžlys, M. N. Shneider, and A. Baltuška, J. Phys. B: At., Mol. Opt. Phys. **48**, 094016 (2015).
[25] H. M. von Bergmann and V. Hasson, J. Phys. D: Appl. Phys. **11**, 2341 (1978).
[26] T. Zhao, Y. Xu, Y. Song, X. Li, J. Liu, J. Liu, and A. Zhu, J. Phys. D: Appl. Phys. **46**, 345201 (2013).